Different combustion modes caused by flame-shock interactions in a confined chamber with an orifice plate

Haiqiao Wei*[,a], Dongzhi Gao[a], Lei Zhou[a], Dengquan Feng[a], Rui Chen[a,b]

[a] State Key Laboratory of Engines, Tianjin University, Tianjin 300072, China

[b] Department of Aeronautical and Automotive Engineering, Loughborough university, LE11 3TU, United Kingdom

Submitted to: **Combustion and Flame**

Article type: **Full Length Article**

*Corresponding author: Haiqiao Wei

Address: 92 Weijin Road, Nankai District, Tianjin, P. R. China

Tel.: +86-22-27402609

Email: whq@tju.edu.cn

Abstract

The present work investigates the interaction of the turbulent flame and shock wave as well as the end-gas autoignition in a newly designed constant volume combustion chamber equipped with an orifice plate using a stoichiometric hydrogen-air mixture. Detailed high speed schlieren photography is used to track the turbulent flame fronts and shock waves which are generated by the laminar flame passing through the orifice plate. The different propagation speeds of the turbulent flames and shock waves can be obtained by controlling the initial pressures and the hole size of the orifice plate. In this work, three combustion modes were obtained clearly by experiment, depending on the interactions of the turbulent flame and shock wave, such as normal combustion, oscillating combustion and end-gas autoignition. The normal combustion is a weak turbulent flame propagation without an obvious shock wave in the confined chamber. The oscillating flame propagation is generated by the interaction of the reflected shock wave and flame front and this process can be clearly visualized in the present work. The end-gas autoignition is induced by the combined effect of the supersonic flame and the shock waves. The accelerating combustion in the confined chamber could produce the primary shock wave and the subsequent secondary shock wave is induced by the secondary flame occurring between the primary flame and primary shock wave. It is found that the secondary shock wave with speed of 780 m/s is faster than the primary one, which is the source of the end-gas autoignition. It is also observed that quasi-detonation wave produced by the end-gas autoignition can reach the speed of 1700 m/s. This wave is accompanied by a strong pressure oscillation which can explain the mechanism of engine knock.

Keywords: Flame-shock interaction; Autoignition; Pressure oscillation; Engine knock;

1. Introduction

Recently the energy crisis and environmental pollution have obliged engine manufactures to realize higher thermal efficiency and lower emissions to meet stringent laws [1]. With this background, many energy-saving technologies have been put forward and as one of the most potential technologies, engine downsizing with supercharging has been followed with interest due to its significant advantages in light weight and compactness. Knock is an inherent constraint on the performance and efficiency of downsized spark ignition (SI) engines since it limits the maximum compression ratio that can be used with any given fuel [2-5]. There is no general agreement on the precise mechanism of engine knock. Two theories have been advanced to explain the origin of knock: the end-gas autoignition theory and the detonation theory [6]. It is generally agreed that knock is caused by the extremely rapid energy release of the end-gas ahead of the propagating turbulent flame, resulting in high local pressures. The irregular form of this pressure distribution causes pressure waves or shock waves to propagate

across the chamber, which causes the chamber to resonate at a certain frequency. Super knock is a new engine knock mode found in downsized spark ignition engines. It can lead to a very high peak pressure (~300 bar) and pressure oscillation (~100 bar), which could damage the cylinder or piston in one engine cycle. It is generally accepted that super-knock originates from pre-ignition and is accompanied by the phenomenon of detonation [7-9]. Essentially, engine knock and super knock are always accompanied by interactions of flame and shock waves and rapid chemical energy release [10-13] or a process in which a part of or all of the charge may be consumed at extremely high rates. Thus, it is important to investigate the interactions of flame and shock waves which are the key to revealing the mechanism of knock and super knock for modern SI engines. The aim of this work is to investigate the flame-shock interactions and the pressure oscillation in a newly designed combustion chamber.

In the literature, there are extensive fundamental studies on the interaction between flame and acoustic wave or shock wave [14-24]. The study of the flame-acoustic wave (pressure wave) interaction has made substantially contribution to understand the flame propagation and flame configuration. These studies experimentally and numerically investigated the dynamics of a distorted tulip flame or folding flame in a tube. In [18-20], the pressure wave is triggered by the contact of flame front with the lateral walls. They made the conclusion that the interaction of flame and pressure wave or acoustic wave leads to the oscillation of the flame front periodically and the different stage of flame propagation and different flame configurations. However, the pressure wave or acoustic wave cannot be directly observed experimentally. Moreover, significant progress in studying the interaction of flame and shock waves with flame acceleration using optical diagnostic techniques has been made owing to recent advances in experiment technology. It was usually investigated in an obstructed, square-cross-section channel [23-27]. In fact, the flame acceleration and propagation are also the most important stages in the interaction between the flame and shock wave for understanding pressure oscillations. A great deal of effort[25, 28-32] has been spent on studying the turbulent flame acceleration mechanism in channels equipped with and without obstacles in past decades. These studies are focused on the stage of flame acceleration governed by flame-shock interaction which is an efficient way of increasing the flame energy release rate to form the detonation. However, the effect of reflected shock wave to flame propagation, end gas autoignition and violent in-cylinder pressure oscillation in confined space have not been discussed in detail.

Most recent evidence indicates that knock or super knock originates from the spontaneous ignition of one or more local regions within the end-gas. Many experiments have been made in a rapid compression machine (RCM) [33-35] as well as in an optical engine withstanding high pressure [11, 12] to prove that the autoignition and detonation phenomenon is present in the end region of the chamber when knock and super knock occurs. The

resulting speeds of the detonation flame in the range of 1500-2300 m/s are close to Chapman-Jouget (CJ) velocity. These results indicate that knock or super knock may be trigged by the end gas autoignition, however, during their experiments, no direct visualization of flame-shock interaction, especially turbulent flame-shock interaction, was observed clearly. And the generation process of end gas autoignition was not directly observed. In summary, the mechanism of flame-shock interaction, autoignition phenomenon as well as pressure oscillation in closed combustion chamber is not adequately understood.

The purpose of this work is to provide further understanding of the flame-shock interactions and end-gas autoignition with induced strong pressure oscillation in confined space, which also could gain an in-depth insight into the mechanism of knock formation. Therefore, a newly designed experimental apparatus equipped with an orifice plate is employed to generate the accelerated turbulent flame and shock wave in this work. The initial turbulent flame is formed rapidly as the laminar flame is passing through the orifice plate. The different propagation speed of the turbulent flame and shock wave can be obtained by controlling the initial pressure and the hole size of the orifice plate. The main new contributions of this work were the observations of three important combustion phenomena and their related pressure oscillations due to flame-shock interaction in confined space using our newly designed experimental apparatus. And the relationship of oscillating intensities of pressure with combustion modes were well demonstrated in this work. The interaction between the flame front and shock wave is imaged by high-speed schlieren photography. The effect of the reflected shock wave on the flame front and consequently on the formation of autoignition are studied in detail. Finally, it has been observed that there are mainly three combustion modes depending on the interaction of turbulent flames and shock waves such as normal combustion, oscillating combustion and end-gas autoignition. The flame propagation velocity of high hydrocarbon fuels such as gasoline is slow and it is hard to form the shock wave by the flame across the orifice plate under present experimental conditions and the end-gas autoignition does not occur. Thus, we selected a stoichiometric H_2-air mixture as the test fuel because of its high flame propagation velocity [28,29] and the formation of the obvious shock wave ahead of the flame front, which can be used to investigate the interactions of flame-shock wave. Under certain conditions, the flame-shock interaction can generate end-gas autoignition resulting in strong pressure oscillation which is similar with what occurred in the SI engine. On the other hand, H_2-air mixture has been studied as a test fuel to study the end gas autoignition in rapid compression machine in the work by Kawahara [11, 12].

The paper is organized as follows: the experimental setup and conditions are briefly discussed in Section 2. Section 3 illustrates the process of flame propagation as the flame passes through the orifice plate. The results and

discussion are presented in Section 4, involving the three different combustion modes of normal combustion, oscillating combustion and end-gas autoignition as well as the analysis of pressure oscillations. Finally, major conclusions from this work are drawn in the last section.

2. Experimental setup and conditions

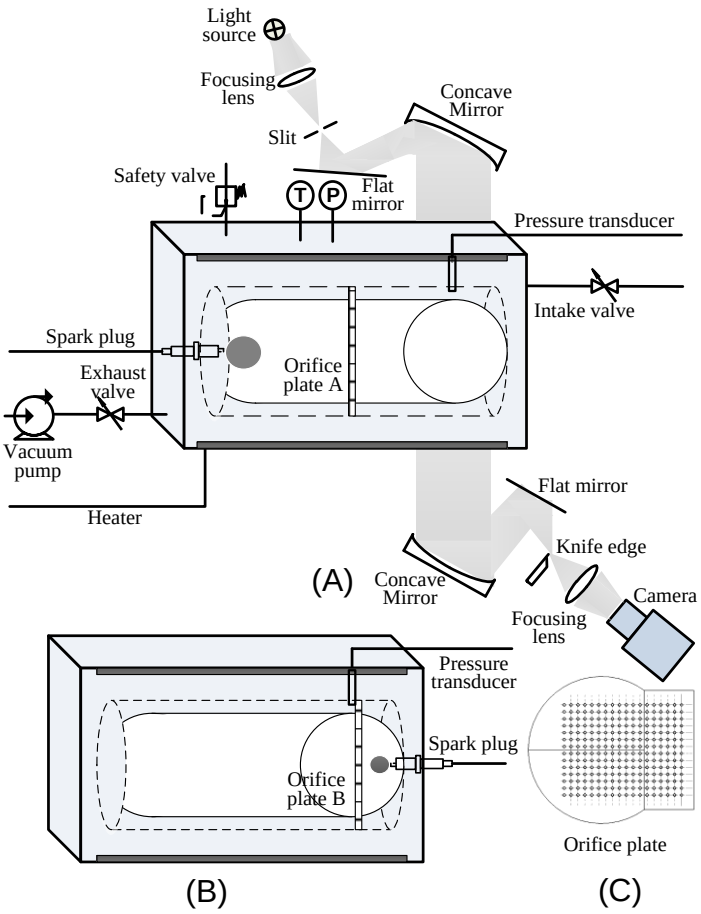

Fig. 1. Schematic diagram of the experimental setup.

Experiments were carried out in a newly designed constant volume combustion bomb equipped with a high-speed schlieren photography system, as shown in Fig. 1. The entire experimental system consists of a constant volume combustion chamber, a high-speed schlieren photography system, a pressure recording system, a temperature control system, an intake and exhaust system, a high-voltage ignition system and a synchronization controller. The combustion chamber is a closed cylindrical cavity with an inner diameter of 100 mm and volume of 2.32 L. It is placed horizontally as shown in Fig. 1. Two windows respectively are mounted on the front and back walls of the combustion chamber. The windows are made of high-quality quartz glass, which can provide optical access with a thickness of 100 mm and 50 mm, respectively. The front window is of a racetrack-shape of 230 mm in length and 80mm in width and the back window a circular one of 80 mm in diameter. The bomb is capable of withstanding a maximum transient pressure of 10 MPa. As a precaution, there is a safety valve with

limit pressure 8 MPa. At the top and bottom of the CVCB, there is a heating plate with a power of 1000 W to heat the bomb to the target temperature uniformly. It is possible to regulate the temperature with a PID controller. The replaceable orifice plate with a different hole size can be installed at the middle (A) and 30 mm (B) distance from the left wall to generate a turbulent flame with a different intensity. The structure of the orifice plate is shown in Fig. 1C. It is made of a 3 mm thick stainless steel plate. There are 252 holes in it, distributed in a matrix structure (18 rows, 14 columns). At positions of A and B, there are two grooves with the width of 3.1 mm and the depth of 3.1 mm on the inner-wall of the combustion chamber to install the orifice plate. The orifice plate is divided into three parts in order to mount easily. The intake and exhaust system are installed at opposite ends of the chamber for scavenging the exhaust gas. High-speed Schlieren photography is a measuring tool widely used for analyzing heat conduction, shock wave, pressure wave, combustion, and explosion, etc. Minor change of density field can be identified with it. A high-speed video camera (Photron FASTCAM SA-Z) is employed, at a shooting speed of 210,000 frames per second. The exposure time is 1 μs. The schlieren system is arranged in a standard Z configuration to observe the turbulent flame and shock wave propagation after passing thorough the orifice plate. The parallel light reflected by the collimator enters combustion chamber from the front window, passes through the end gas region of the chamber, and comes out from the back window. And then the light is reflected by the schlieren head, cut by the knife edge and entered into the high-speed video camera. The spark plug is arranged on the left wall of the combustion chamber for condition A and on the right wall for condition B. The pressure transducer (Kistler 6113B at 100 kHz) is located on the top wall at the distance of 35 mm to the left wall. More detailed of the experimental specifications can be found in reference [36, 37].

Initially, the combustion chamber is heated up to the target temperature by the temperature control system. The H_2-air mixture is obtained by the partial pressure method. The test conditions are shown in Table 1. Before igniting, the H_2 and air mixture is initially premixed for 2 minutes to achieve the homogeneous mixture at the target condition of initial temperature 353K. At last, the spark igniter, pressure recorder and high-speed digital video camera are triggered simultaneously by the synchronization controller. In this study, the uncertainty measures for initial pressure and temperature are no more than 0.05 bar and 2 K, respectively.

Table 1 Experimental conditions.

Experiment	Position of orifice plate and spark plug	Hole size/mm	Initial pressure/bar	Initial temperature/K
Different combustion modes in the end of the chamber	A	1.5, 3	1, 1.5, 2, 2.5	353

The process of flame acceleration	B

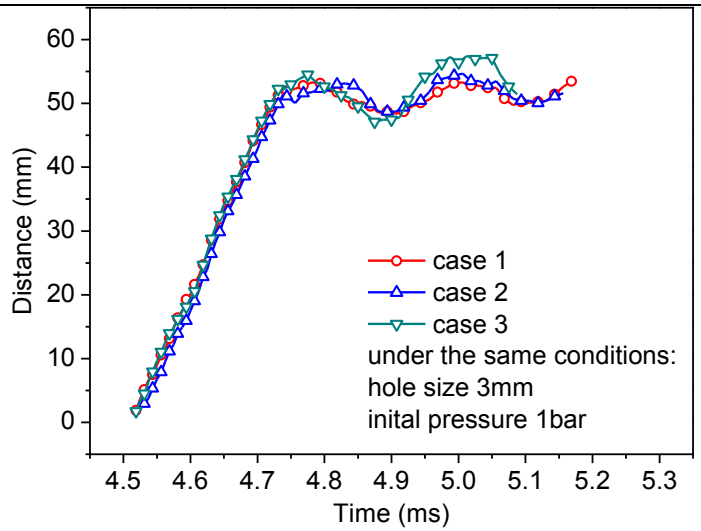

Fig. 2. Repeatability test.

In order to verify the repeatability of the test device. Three cases of turbulent flame position versus time conducted in setup A under the same conditions (hole size of 3mm, initial pressure of 1bar) were shown in Fig. 2. The tendencies of flame trajectory in three cases are consistent with each other. The relative error does not exceed 5% and this is acceptable for high-speed turbulent flame propagation after the orifice plate. Thus, the experimental setup for this test is reliable.

3. The process of flame acceleration passing through the orifice plate

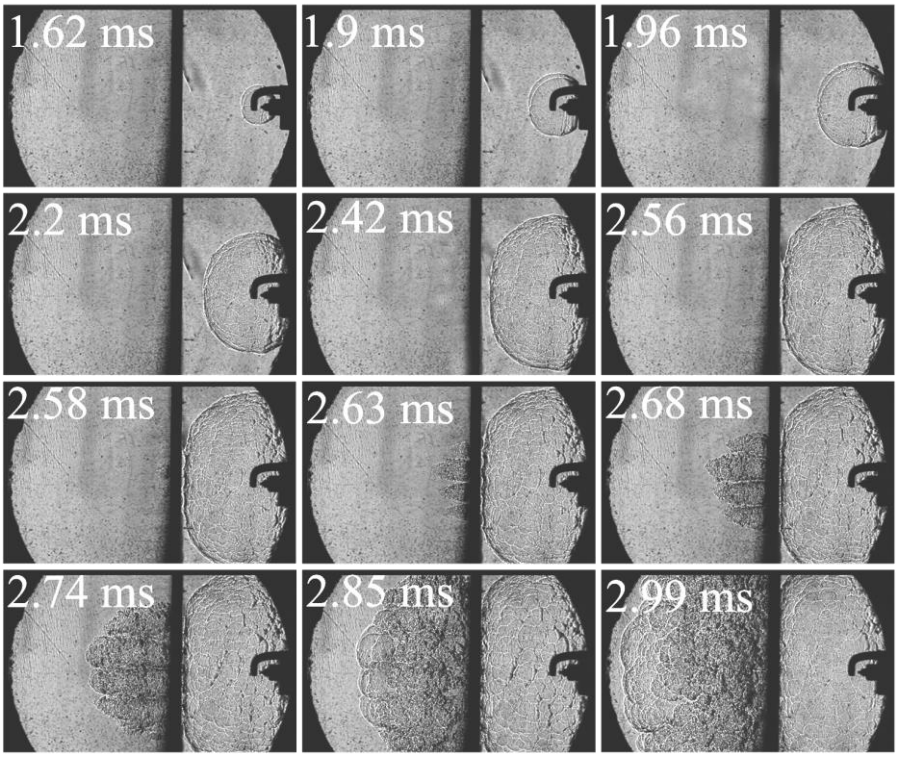

Fig. 3. Chronological schlieren images for flame acceleration passing through orifice plate B.

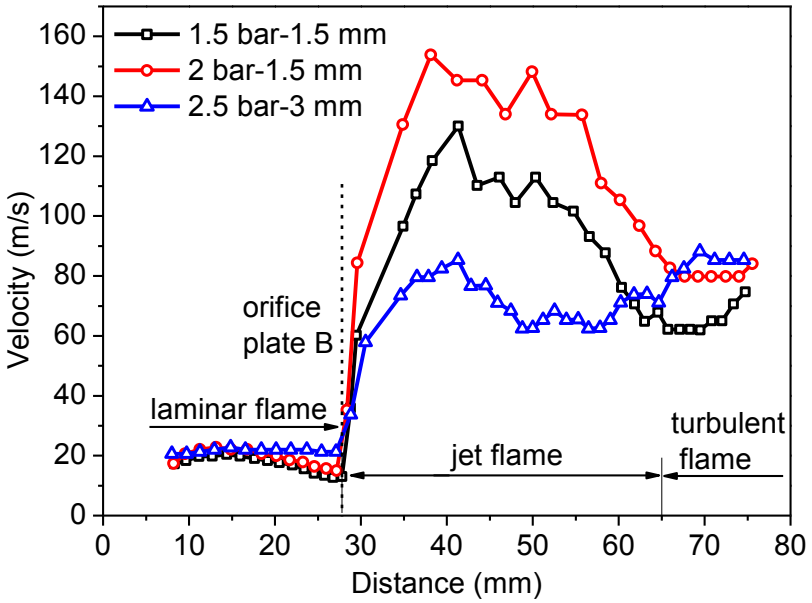

Fig. 4. The velocities of flame front propagation at different initial pressures and hole sizes.

The flame acceleration process is investigated by the confined chamber equipped with orifices plate B as shown in Fig. 3. These images are obtained at the conditions of an initial pressure of 2.5bar and a hole size of 3mm. The orifice plate is located at place B so that the process of flame acceleration can be observed by the high-speed schlieren photography. Fig. 4 shows the curves of flame velocity passing through orifice plate B and the three conditions in this section are related to the results in the following. After spark plug discharging, an outwardly propagating spherical flame is formed with a stretched flame propagation speed of 20 m/s at an initial pressure of 2 bar as shown in Fig. 4. The flame velocity declines slightly before passing through the orifice plate due to the resistance of orifice plate. Meanwhile, the flame surface becomes a cellular structure because of the diffusional-thermal and hydrodynamic instability [38, 39] as shown in Fig 3 at 2.42 ms, which is a well-known phenomenon. When the flame passes through the orifice plate B, the area of the flame brush is increased and the jet flame appears.

The combustion reaction is promoted to accelerate the spread of turbulent flame at time of 2.68ms as shown in Fig. 3 and there is a sharp flame acceleration leading to the formation of a robust turbulent flame. The flame has a speed of 150 m/s at an initial pressure of 2 bar and a hole size of 1.5 mm, as can be seen in Fig. 4. The effects of hole size and initial pressure on flame propagation speed are significant. Comparing the conditions of 1.5 bar and 2 bar at the same hole size, the flame propagation velocity increases with the increase of initial pressure，because there is a higher energy density under higher initial pressure. On the other hand, the flame crossing orifice plate with small a hole size leads to a large increase of the flame surface and stronger flame instability than that with

large hole size. As the flame leaves the orifice plate, the jet flame velocity decreases. However, at the end region of the observation window from 65mm to 75mm, turbulent flame propagation velocity tends to increase. Because at the end region the turbulent flame forms and the flame self-acceleration continues to drive the flame-front velocity increase. In previous work [40, 41], the flame self-acceleration has been validated. The present result is in line with the Bychkov theory [25] on flame acceleration mechanism over obstacles. Moreover, Benedetto et al. [28-30] used time-resolved particle image velocimetry (TRPIV) and large eddy simulation (LES) to investigate the unsteady flame propagation around toroidal vortices generated at the wake of a circular orifice. Their simulation results showed the trend of flame propagation.

4. Results and discussion

As discussed in Section 3, there is a significant acceleration as the flame passes through the orifice plate B. In order to study the combustion mode in the end gas of the confined chamber, the orifice plate is installed at position A to generate a different intensity of turbulent flame. The following study with hydrogen-air mixtures focuses on the interactions of turbulent flame and shock wave at the end of the closed chamber and three different combustion modes such as normal combustion, oscillating combustion and end-gas autoignition. In addition, the cylinder pressure histories are also studied as follows.

4.1 Normal combustion without shock wave formation (Mode 1)

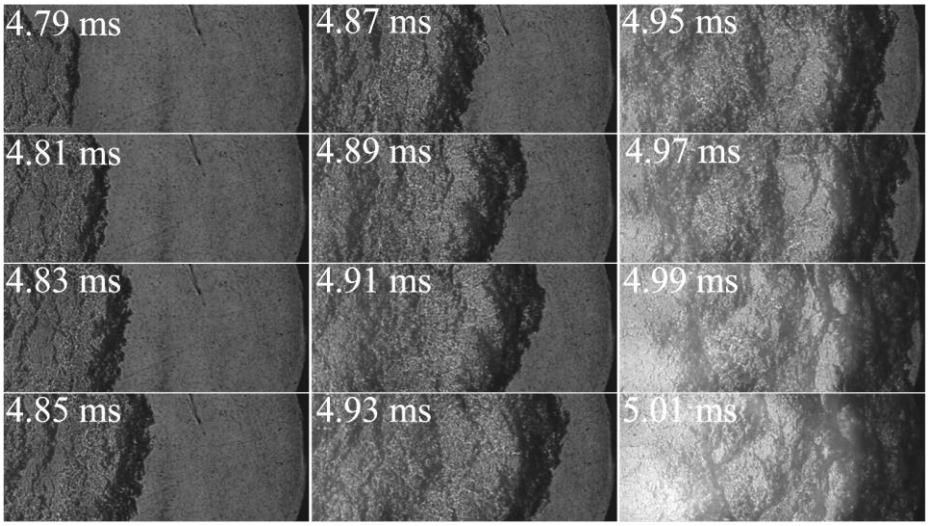

Fig. 5. Flame propagation images at initial pressure of 1.5 bar and hole size of 1.5 mm with orifice plate at position A.

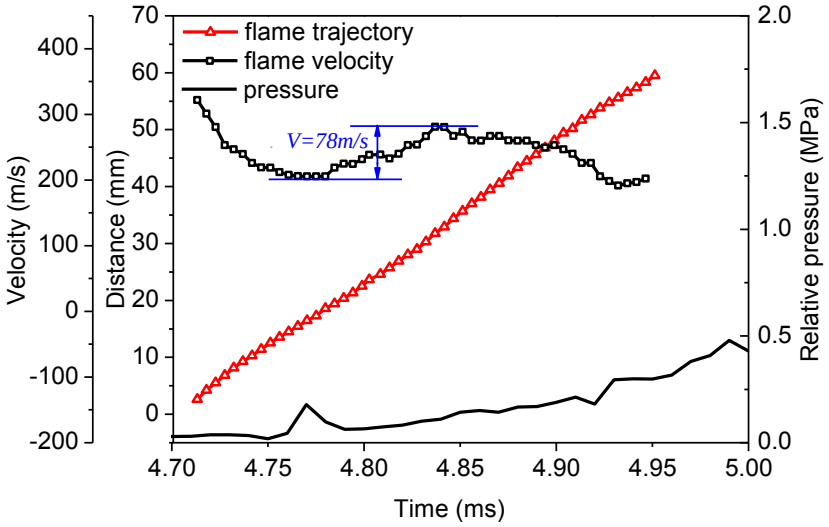

Fig. 6. The profiles of flame front trajectory, velocity and pressure variation in the chamber obtained at an initial pressure of 1.5 bar and a hole size of 1.5 mm.

Figure 5 shows a time-sequence of flame propagation images at an initial pressure of 1.5 bar and a hole size of 1.5 mm. The flame propagation velocity is calculated from the time derivative of the flame tip location. It is worth saying that the right edge of the images is the end wall of the combustion chamber. As shown in Fig. 5, the turbulent flame propagates to the right of the chamber smoothly. The flame trajectory is almost linear with time presented by the triangle in Fig. 6. There is no shock wave formed ahead of the flame and the turbulent flame velocity is about 250 m/s less than the local speed of sound (385.16 m/s in the unburned mixture at temperature 353K). The profile of the flame velocity in this process was shown in Fig. 6. And there are slight fluctuations with an amplitude of 78 m/s, which is smaller than what is shown in Fig 8b. This is due to the interaction of the flame front with the pressure wave or acoustic wave [18-20], triggered by flame acceleration and reflected by the walls. The transient pressure rises smoothly except for one or two small peaks throughout this process and the pressure amplitude is small. That means that the flame propagation in the end of the combustion chamber is almost steady when there are no flame-shock interactions.

4.2 Oscillating combustion with flame-shock interaction (Mode 2)

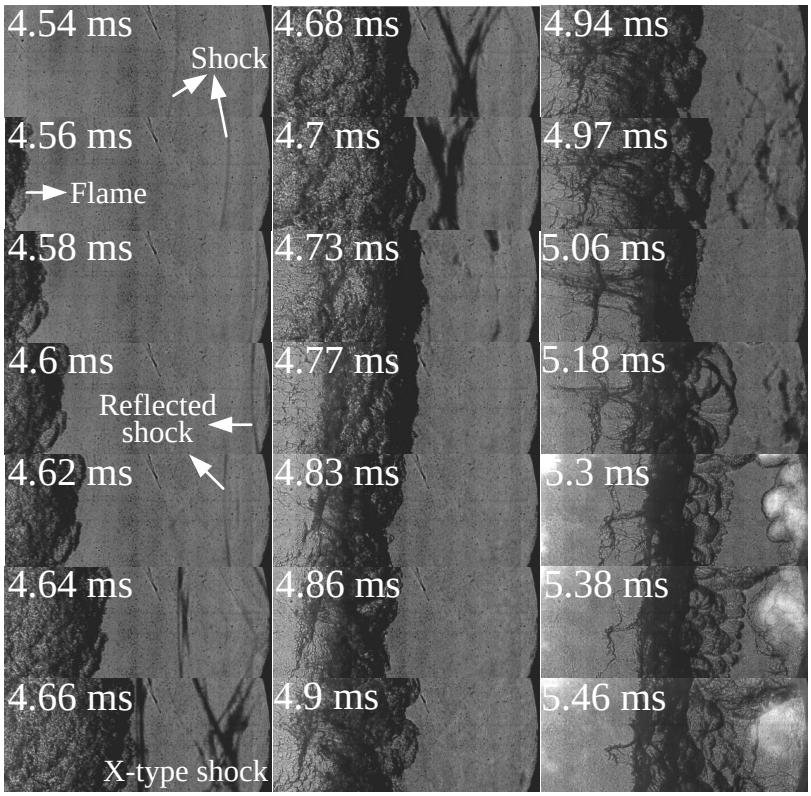

Fig. 7. Flame and shock wave interactions at an initial pressure of 2.5 bar and a hole size of 3 mm with orifice plate at position A.

When flame propagates along the combustion chamber passing through the orifice plate, there will be an acceleration process. According to aerodynamics, the compression waves ahead of the flame coalesce and form a strong shock wave [42]. This shock can be visualized clearly by high-speed schlieren photography in present work. Fig. 7 illustrates the development of the turbulent flame propagation and shock wave, meanwhile the interaction of flame with the reflected shock wave. There is an obvious shock wave with the speed of roughly 500 m/s formed ahead of the accelerating turbulent flame with the speed of roughly 300 m/s at 4.5ms in the initial stage of the test window as shown in Fig. 8b. It is observed that the turbulent flame velocity obtained in end gas region is fluctuant. As the shock wave reaches the end wall of the combustion chamber at about 4.58ms as shown in Fig. 7, an obvious reflected shock wave is produced at 4.6ms. Subsequently, the obvious interaction of flame and reflected shock wave starts at 4.66ms. An X-shape shock appears, which is generated by shock coalescing from the top and bottom wall of the chamber. Thus, the flame front is pushed back and spreads reversely due to the impact of several reflected shock waves at 4.86ms. This leads to the oscillating combustion in the end gas of the combustion chamber. On the basis of Taylor instability theory, Markstein [43] suggested that this flame inversion is caused by the velocity field (drastic velocity decrease) behind the shock wave as it passes the flame. A drastic change in the unburned gas velocity is produced by the shock wave effect, causing violent velocity decrease and reverse flow in

the unburned region. The shock wave acts as a source of disturbance, leading to velocity change in the unburned mixture.

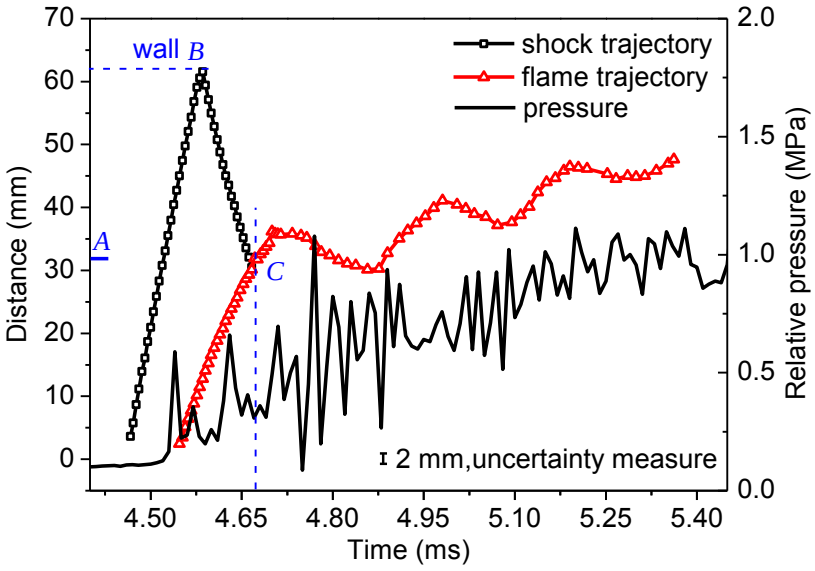

(a)

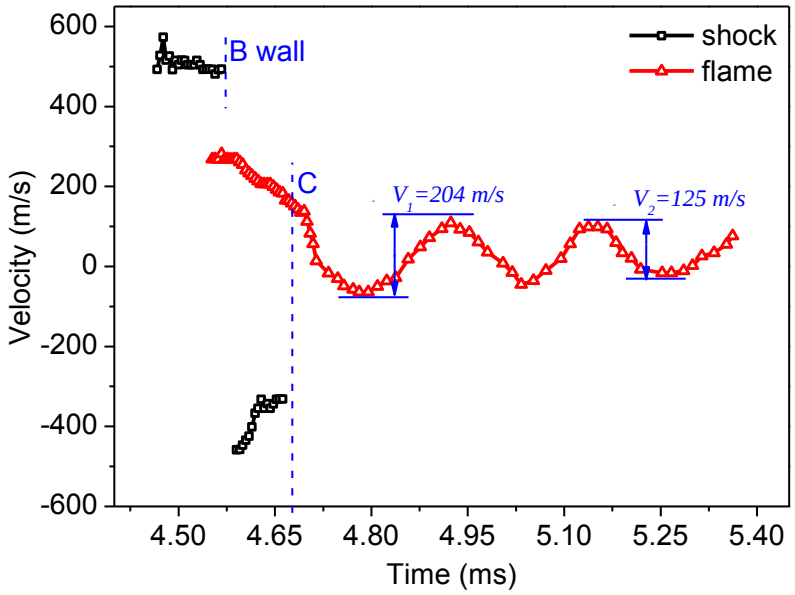

(b)

Fig. 8. The profiles of the distance, pressure (a) and velocity (b) versus time at an initial pressure of 2.5 bar and a hole size of 3 mm (A, position of pressure transducer; B, the end wall of chamber; C, the intersection point of reflected shock wave and flame).

Shown in Fig. 8a are the trajectories of the shock wave and the leading edge of the turbulent flame brush as well as the pressure profile. The velocities of shock wave and flame versus time are shown in Fig. 8b. The trajectory of the shock wave versus time is almost linear relationship and it is divided into two sections with different slopes by position B (the wall in the end region of the combustion chamber) as shown in Fig. 8a. This

indicates that the velocities of the forward shock and reflected shock are constant. The velocity of forward shock is roughly 500 m/s which larger than local sound speed. After reflected, the velocity of shock wave is reduced to about 420 m/s as shown in Fig. 8b. This indicates that the power of the reflected shock wave reduces due to the dissipation of energy. The intensity of reflected shock wave decreases with time and the velocity slows down to about 320 m/s when it contacts with the flame front at point C as shown in Fig. 8a. After the flame and shock wave interaction occurs, flame velocity decreases with time and reaches a minimum value of -84 m/s (the negative value indicates reverse propagation) at the time of 4.77ms. Then the velocity increases and reaches a maximum value of 120 m/s at the time of 4.93 ms induced by the Richtmyer-Meshkov (R-M) instability [44] and turbulent flame self-acceleration [45]. The flame surface is increased by the acoustic wave or reflected shock wave due to R-M instability, which leading to increasing of turbulent flame according to turbulent flame self-acceleration characteristic. The amplitude of the flame speed oscillation is 204 m/s which is three times larger than that in Fig. 6. It is worth noting that the flow field caused by shock wave will be reflected back and forth several times between the left wall and the right wall of the combustion chamber. Thus the trajectory and velocity of the flame in the combustion chamber change up and down several times as shown in Fig. 8. The amplitude of fluctuation is reduced with time, which indicates that the power of reflected shock waves and the flow field caused by them are weakened with the number of reflections. Finally, the flame maintains the forward trend to the end and burns the whole chamber at about 5.46ms. It should be noted that the oscillation frequency of the flame front is consistent with the frequency that the shock wave reflects back and forth in the combustion chamber. As shown in Fig. 8a, the pressure accompanying flame-shock interaction phenomenon in this case has a maximum amplitude of 0.51 MPa which is larger than that shown in Fig. 6. However, its frequency is significantly larger than that of flame speed oscillation. This is mainly because the cylinder pressure signal contains the information of all types of pressure waves from different orientations in confined space. But the oscillating flame propagation is mainly caused by the transverse shock wave in the combustion chamber. Therefore the frequency of flame oscillation is consistent with the frequency of shock wave reflected back and forth in the combustion chamber.

4.3 End-gas autoignition with flame-stronger shock interaction (Mode 3)

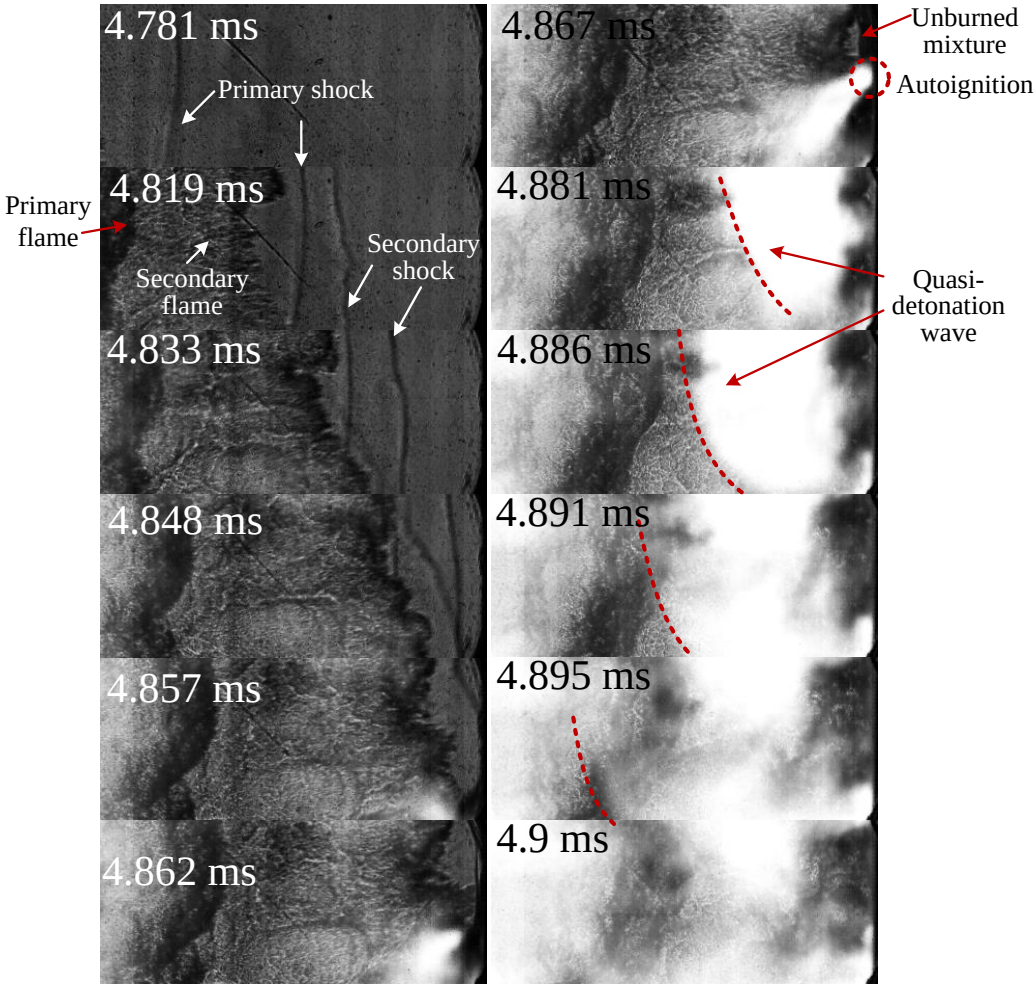

Fig. 9. Sequence of high-speed schlieren images of end-gas autoignition with an initial pressure of 2 bar and a hole size of 1.5 mm with orifice plate at position A.

One of the important observations in present work is the end-gas autoignition induced by strong flame-shock wave interactions. Fig. 9 shows a sequence of high-speed schlieren images of the development of turbulent flames and shock waves, as well as the end-gas autoignition in the closed chamber at the conditions of an initial pressure of 2 bar and a hole size of 1.5 mm. The development of the flames and the process of end-gas autoignition induced by the combined effect of supersonic flame and the reflection of shock waves are investigated in this section. Firstly, the primary shock ahead of flame front can be seen clearly at 4.781ms. Then, the primary flame enters the observation area at 4.819ms and the secondary flame occurs between the primary flame and primary shock. The secondary shock induced by the secondary flame can be observed in front of the primary shock and has a maximum propagation velocity of 750m/s. This is mainly because the temperature of the unburned gas increase transiently after the primary shock wave propagation. On the other hand, the unburned mixture is also heated by the thermal radiation of the primary flame. Because the appearance of a wrinkle leads to an increase in flame surface and consequently induces a more intense secondary flame in burning rate. The flames and shocks in

this case propagate in the same direction toward the end of the combustion chamber. The distance between them is close and there are no flame and reflected shock interactions which are different from the example shown in Section 4.2. The secondary shock wave spread faster than the primary and ahead of it as shown in Fig. 9 at 4.833ms. The secondary shock wave propagates to the end wall of the combustion chamber and spreads inversely due to reflection. The unburned mixture near the end wall is affected by the shock wave twice and its physical states change dramatically, the pressure, temperature and density are increased instantaneously. At 4.867ms, autoignition occurs near the end wall of the chamber and a bright quasi-detonation wave propagating rapidly with the speed of 1700 m/s is formed. The peak value of in-cylinder pressure reaches 4.7 MPa, accompanying a substantial energy release instantaneously. The entire sequence of frames is shown in Video 2 in supplement materials.

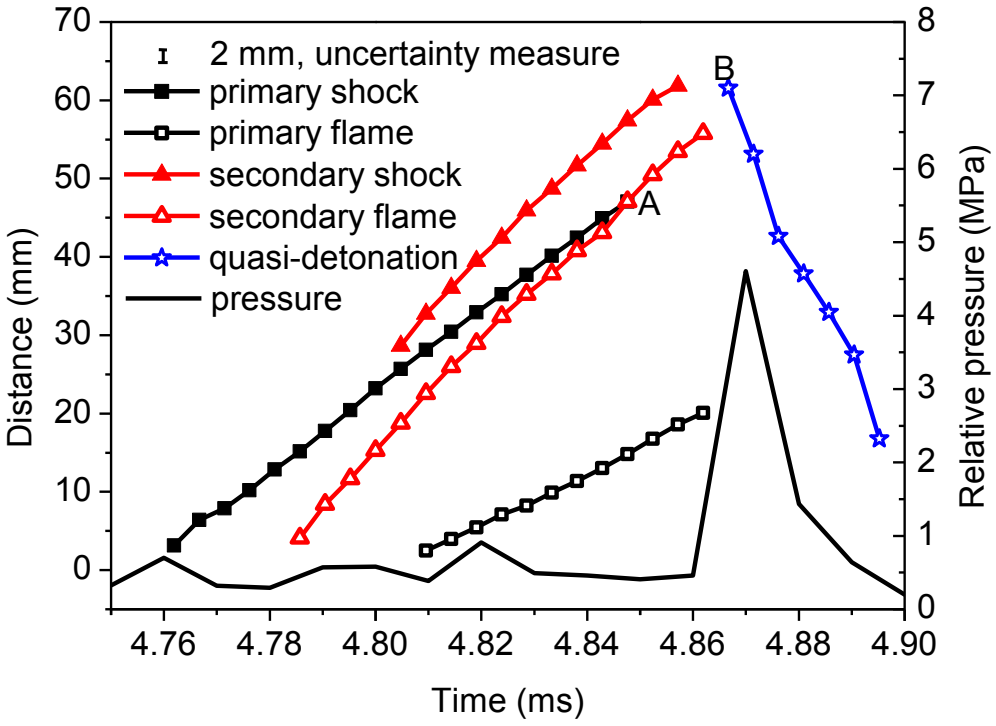

(a)

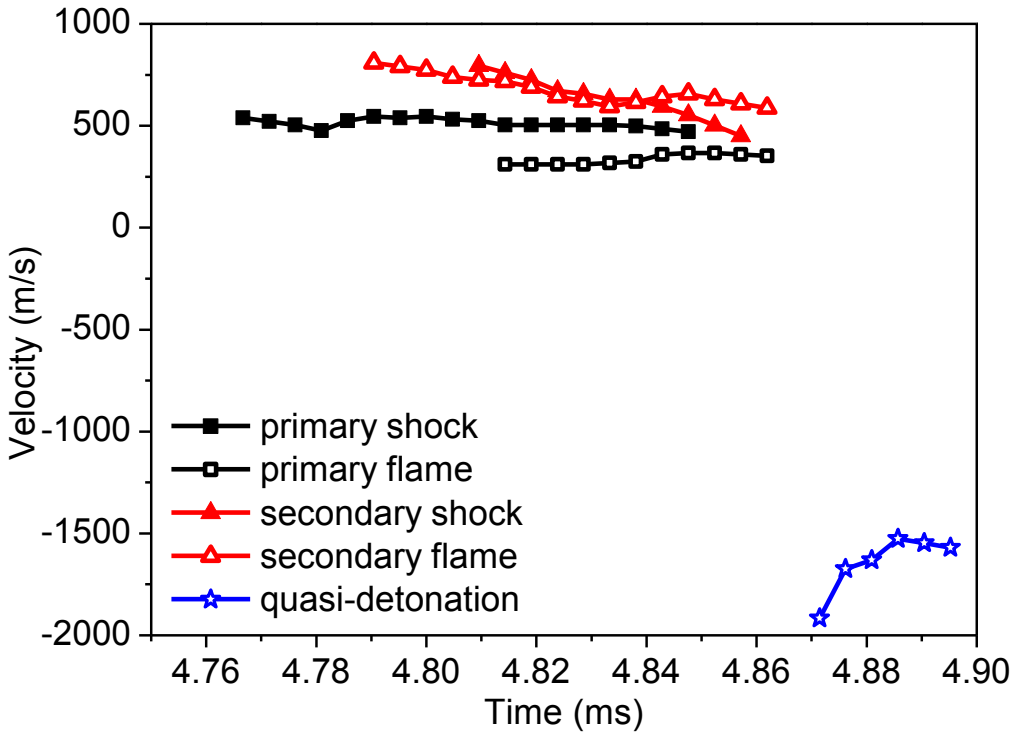

(b)

Fig. 10. The profiles of the distance, pressure (a) and velocity (b) versus time corresponding to Fig. 7 at an initial pressure of 2 bar and a hole size of 1.5 mm (A, the intersection of the secondary flame and primary shock; B, the position of autoignition).

The trajectories of the shock waves and the turbulent flames as well as the pressure history are shown in Fig. 10a. Fig. 10b shows the velocities of flames and shocks as well as the quasi-detonation wave at an initial pressure of 2 bar and a hole size of 1.5 mm. Note that the two flames and two shock waves as shown in Fig. 9 can be clearly distinguished from the slope of velocity as shown in Fig.10a. The secondary flame and secondary shock have greater slopes (velocities) than their primary countparts. As can be seen from Fig. 10b, the velocities of the secondary flame and secondary shock wave are greater than the primary ones and their values are 750, 780, 370 and 500 m/s respectively. Position A represents the intersection of the secondary flame and the primary shock wave. The end-gas autoignition occurs at position B at about 4.867ms. When the shock wave generated by flame acceleration is strong enough, a secondary flame is formed between the primary flame and primary shock and its velocity can reach 750 m/s, which is faster than the 370 m/s of the primary flame as shown in Fig. 9 and Fig. 10b. The secondary shock wave induced by the secondary flame propagates faster with a velocity of 780 m/s. The high speed of flames and shock waves can be maintained as shown in Fig. 10b due to the interactions of flame and shock waves where turbulent flame can drive the shock wave and the shock wave will promote flame acceleration. This is different from the oscillating combustion introduced in Section 4.2. The secondary flame and shock wave

produce a strong compression effect on the end gas and consequently the end-gas autoignition occurs at a higher temperature and pressure induced by the obvious shock wave. A quasi-detonation wave is then formed propagating reversely with a propagation velocity of 1700 m/s. And it leads to a peak pressure of 4.5MPa which is higher than those cases without autoignition as discussed before. This is detrimental and results in a powerful gas explosion [46]. The pressure fluctuates significantly with a large amplitude of 3.45Mpa as shown in Fig. 12 which is 7 times higher than the pressure of oscillating combustion.

4.4 Pressure oscillation at different combustion modes

Table 2 Flame front and shock velocities in different combustion modes.

Combustion modes	Flame velocity	Shock velocity	Autoignition in the end region
Normal combustion	Average velocity: 250m/s Amplitude: 78m/s	None	None
Oscillating combustion	Average velocity: 50m/s Amplitude: 204m/s to 125m/s	Forward shock: 500 m/s Reflected shock: ~ -400m/s	None
End-gas autoignition	Primary flame velocity: 370m/s Secondary flame velocity: 750m/s	Primary shock velocity: 500m/s Secondary shock velocity: 780m/s	~1700m/s

As discussed above, three combustion modes can be obtained due to the different intensities of flame and shock wave in present work and the associated velocities are summarized in Table 2. It can be concluded that the combustion modes are related to the flame front propagation and shock velocities. The flame velocities in the end of the closed chamber are oscillating with different amplitude of 78m/s for normal combustion and 204m/s for oscillating combustion. As end-gas autoignition, the flame spreads to the end with constant velocity of 750m/s and fluctuations in flame speed does not occur. As can be seen, the average flame velocity of oscillating combustion is 50m/s which is smaller than the 250m/s of the normal combustion. This is because the influence of reflected shock on flame velocity is significant. The secondary shock reflects by the end wall of the combustion chamber and leads to end-gas autoignition since it is strong enough with the speed of 780m/s. According to gas dynamics, autoignition occurs after the shock has hit the wall and is reflected because compression and temperature are largest. Then autoignition kernel forms near the wall from a powerful flame which drives the reflected shock wave. Thus form a quasi-detonation combustion with the velocity of 1700m/s which leads to extremely high pressure spikes. In this case, the cylinder pressure has a large amplitude of fluctuation as discussed in the following.

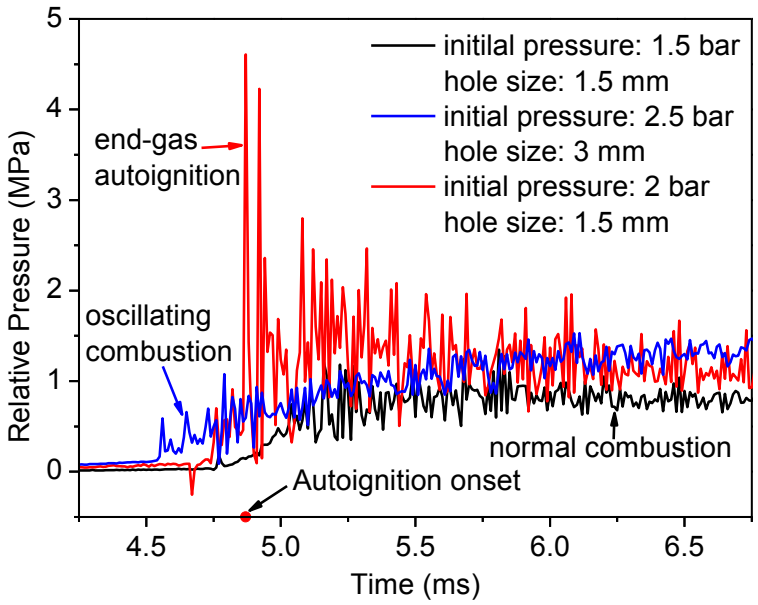

Fig. 11. Pressure traces for three combustion modes at different initial conditions.

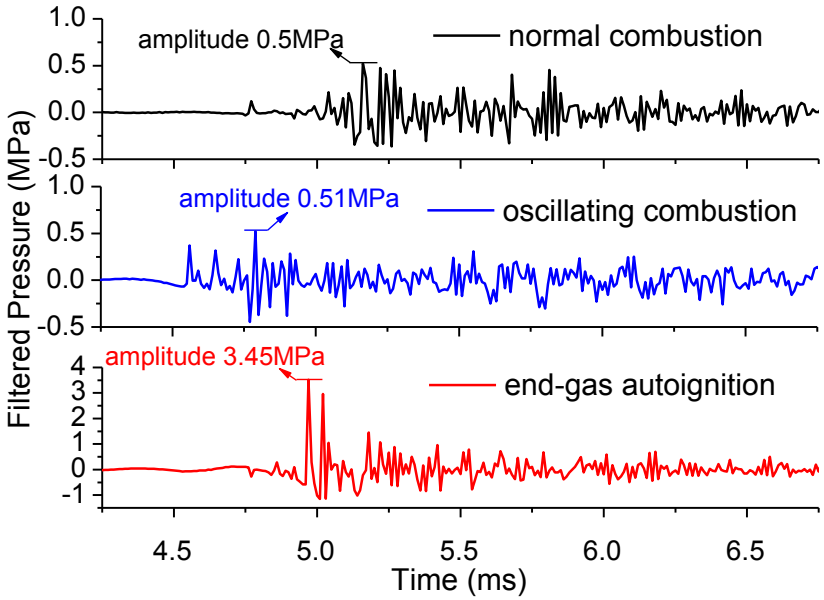

Fig. 12. High-pass filtered pressure for three combustion modes.

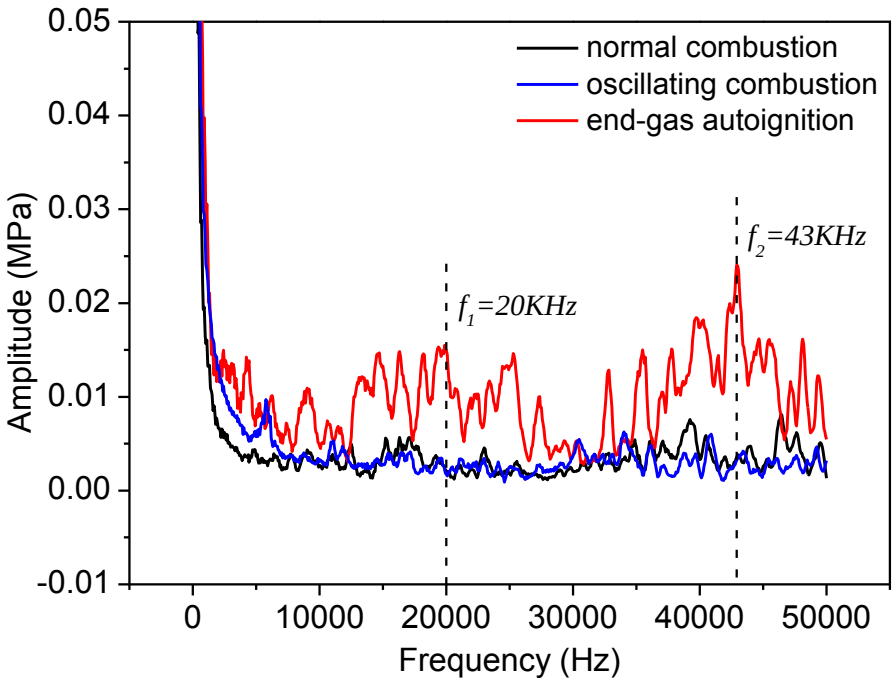

Fig. 13. FFT filtered pressure for three combustion modes.

Figure 11 shows the pressure traces corresponding to different combustion modes presented in Section 4.1-4.3. These results are further processed using high-pass filtering by 20 KHz and Fast Fourier Transform (FFT) analysis as shown in Fig. 12 and Fig. 13, respectively. When there is no shock wave formation, the amplitude of filtered pressure is 0.5Mpa as shown in Fig. 12. As the oscillating combustion mode, cylinder pressure fluctuates with the amplitude of 0.51MPa. This is close to the normal combustion mode without shock wave formation. This indicates that pressure fluctuations occur when the flame propagation speed is greater than normal by only one order of magnitude, even though there is no shock wave and it can be triggered by an invisible pressure wave or acoustic wave [47]. When end-gas autoignition occurs with an initial pressure of 2.0 bar and a hole size of 1.5 mm, high-frequency pressure fluctuations with amplitudes decay versus time are measured. It can be found that the pressure rapidly rises when the quasi-detonation occurs because of the autoignition of the end-gas. The maximum oscillation amplitude can reach 3.45MPa. For end-gas autoignition modes, the frequency obtained by FFT analysis are mainly distributed in 20 KHz and 43 KHz. When autoignition does not occur, the curves associated with combustion mode 1 and 2 are similar, and the partial pressures locate at each frequency uniformly as shown in Fig. 13. This suggests that the frequency of in-cylinder pressure changes because of the combustion mode transition.

According to the current study, the intensity level of shock wave depends on turbulent flame velocity and shock wave which is related to the two factors of the hole sizes that determines the initial turbulent flame formation and initial pressure that determines the turbulent flame propagation velocity. In fact, reducing the hole

size can increase the wrinkled flame surface at smaller scales and the turbulent intensity, which results in a fast flame. Moreover, increasing the initial ambient pressure could increase the turbulent flame propagation velocity [45]. Hence, combined with flame acceleration process as shown in Fig. 4 the shock wave with initial pressure of 2 bar and a hole size of 1.5 mm is the strongest and the end-gas autoignition occurs in this condition. It is also found that there is an earlier pressure fluctuation when the orifice plate of 3mm diameter is used, which indicates that the transmittance of orifice plate has an impact on the pressure. In short, the current study suggests that end-gas autoignition associated with reflected shock wave is the main reason for generating in-cylinder pressure oscillation with high amplitude which is similar to engine knock.

5. Conclusions

Relationship of turbulent flame, shock wave and autoignition in a newly designed confined chamber has been investigated using high-speed schlieren photography and piezoelectric pressure transducer. The interaction phenomenon of the turbulent flame and shock wave inducing to different combustion modes and pressure oscillation is obviously observed by high-speed schlieren photography in this work. The results show that there are different combustion modes in the end of the combustion chamber depending on the interaction of turbulent flames and shock waves, such as normal combustion, oscillating combustion and quasi-detonation due to the end-gas autoignition. Meanwhile, the different combustion modes induced different pressure oscillations.

When there is no shock wave formation, the flame velocity has a slight fluctuations with amplitude of 78 m/s due to the interaction of flame front with the pressure wave or acoustic wave in closed chamber. When there is an obvious shock wave with the speed of roughly 500 m/s formed ahead of the accelerating turbulent flame, the interactions of the flame and reflected shock wave is intense. The flame front is pushed back and spreads reversely by the reflected shock waves. This leads to the oscillating combustion in the end gas of the combustion chamber. The amplitude of the flame speed oscillation is 204m/s which is three times larger than that of normal combustion without any shock wave formation. Noted that the oscillation frequency of turbulent flame propagation is mainly depended on the transverse shock wave in the confined combustion chamber. Essentially, these phenomena are induced by the flow field caused by the shock wave or acoustic wave. And both the amplitude of the high-pass filtered pressure and the frequency of the FFT filtered pressure are similar. When a shock wave with the velocity of 780m/s propagates to the end of the combustion chamber, autoignition occurs near the end wall of the chamber and a bright quasi-detonation wave propagating rapidly with the speed of 1700 m/s is formed. The peak value of in-cylinder pressure reaches 4.7 MPa, accompanying a substantial energy release instantaneously. The pressure fluctuates significantly with a high amplitude of 3.45MPa which is 7 times higher than the pressure of oscillating

combustion due to a rapid chemical energy release.

According to present study, the intensity level of pressure oscillation depends on combustion modes involving turbulent flame velocity and shock wave. The combustion modes are related to the two important factors of the hole size that determines initial turbulent flame formation and initial pressure that influences the turbulent flame propagation velocity. The mechanism of quasi-detonation induced by end gas autoignition in the closed combustion chamber is observed, which is the key to explaining in-cylinder pressure oscillation with a high amplitude during engine knock or super knock.

Acknowledgements

This work was supported by the National Natural Science Foundation of China (Grant No. 51476114). The author would also express his appreciation towards Ph.D. Sotiris Petrakides in Loughborough University for providing valuable comments.

References

[1] J. Rudloff, J.M. Zaccardi, S. Richard, J.M. Anderlohr, Analysis of pre-ignition in highly charged SI: Emphasis on the auto-ignition mode, Proc. Combust. Inst. 34 (2013) 2959-2967.

[2] D. Bradley, G.T. Kalghatgi, Influence of autoignition delay time characteristics of different fuels on pressure waves and knock in reciprocating engines. Combust. Flame 156 (2009) 2307-2318.

[3] A. Misdariis, O. Vermorel, T. Poinsot, LES of knocking in engines using dual heat transfer and two-step reduced schemes, Combust. Flame 162 (2015) 4304-4312.

[4] A. Robert, S. Richard, O. Colin, T. Poinsot, LES study of deflagration to detonation mechanisms in a downsized spark ignition engine, Combust. Flame 162 (2015) 2788-2807.

[5] H. Yu, Z. Chen, End-gas autoignition and detonation development in a closed chamber, Combust. Flame 162 (2015) 4102-4111.

[6] J.B. Heywood, Internal combustion engine fundamentals, McGraw-Hill College, New York, US, 1988, p. 457.

[7] Y. Qi, Z. Wang, J. Wang, X. He, Effects of thermodynamic conditions on the end gas combustion mode associated with engine knock, Combust. Flame 162 (2015) 4119-4128.

[8] M. Pöschl, T. Sattelmayer, Influence of temperature inhomogeneities on knocking combustion, Combust. Flame 153 (2008) 562-573.

[9] Z. Wang, Y. Qi, X. He, J Wang, S Shuai, C.K. Law, Analysis of pre-ignition to super-knock: hotspot-induced deflagration to detonation, Fuel 144 (2015) 222-227.

[10] J. Pan, G. Shu, H. Wei, Interaction of Flame Propagation and Pressure Waves During Knocking Combustion

in Spark-Ignition Engines, Combust. Sci. Technol. 186 (2014) 192-209.

[11] N. Kawahara, E. Tomita, Y. Sakata, Auto-ignited kernels during knocking combustion in a spark-ignition engine, Proc. Combust. Inst. 31 (2007) 2999-3006.

[12] N. Kawahara, E. Tomita, Visualization of auto-ignition and pressure wave during knocking in a hydrogen spark-ignition engine, Int. J. Hydrogen Energ. 34 (2009) 3156-3163.

[13] C. Dahnz, U. Spicher, Irregular combustion in supercharged spark ignition engines-pre-ignition and other phenomena, Int. J. Engine Res. 11 (2010) 485-498.

[14] A.M. Khokhlov, E.S. Oran, A.Y. Chtchelkanova, J.C. Wheeler, Interaction of a shock with a sinusoidally perturbed flame, Combust. Flame 117 (1999) 99-116.

[15] V.N. Gamezo, A.M. Khokhlov, E.S. Oran, The influence of shock bifurcations on shock-flame interactions and DDT, Combust. Flame 126 (2001) 1810-1826.

[16] V.N. Gamezo, A.M. Khokhlov, E.S. Oran, Effects of wakes on shock-flame interactions and deflagration-to-detonation transition, Proc Combust Inst 29 (2002) 2803-2808.

[17] R.K. Zipf, V.N. Gamezo, K.M. Mohamed, E.S. Oran, D.A. Kessler, Deflagration-to-detonation transition in natural gas–air mixtures, Combust. Flame 161 (2014) 2165-2176.

[18] H. Xiao, Q. Wang, X. Shen, S. Guo, J. Sun, An experimental study of distorted tulip flame formation in a closed duct, Combust. Flame 160 (2013) 1725-1728.

[19] X. Huahua, H. Ryan, O. Elaine, Formation and evolution of distorted tulip flames, Combust. Flame 162 (2015) 4084-4101.

[20] X. Huahua, M. Dmitriy, S. Jinhua, M. Vladimir, Experimental and numerical investigation of premixed flame propagation with distorted tulip shape in a closed duct, Combust. Flame 159 (2012) 1523-1538.

[21] A. Petchenko, V. Bychkov, V.y. Akkerman, L.-E. Eriksson, Violent folding of a flame front in a flame-acoustic resonance, Phys Rev Lett 97 (2006) 164501.

[22] A. Petchenko, V. Bychkov, V.y. Akkerman, L.-E. Eriksson, Flame–sound interaction in tubes with nonslip walls, Combust. Flame 149 (2007) 418-434.

[23] G. Ciccarelli, C.T. Johansen, M. Parravani, The role of shock-flame interactions on flame acceleration in an obstacle laden channel, Combust. Flame 157 (2010) 2125-2136.

[24] T. Pinos, G. Ciccarelli, Combustion wave propagation through a bank of cross-flow cylinders, Combust. Flame 162 (2015) 3254-3262.

[25] V. Bychkov, D. Valiev, L.E. Eriksson, Physical mechanism of ultrafast flame acceleration, Phys. Rev. Lett.

101 (2008) 164501.

[26] M.A. Liberman, M.F. Ivanov, A.D. Kiverin, M.S. Kuznetsov, A.A. Chukalovsky, T.V. Rakhimova, Deflagration-to-detonation transition in highly reactive combustible mixtures, Acta Astronaut. 67 (2010) 688-701.

[27] M.A. Liberman, M. Kuznetsov, A. Ivanov, I. Matsukov, Formation of the preheated zone ahead of a propagating flame and the mechanism underlying the deflagration-to-detonation transition, Phys. Lett. A 373 (2009) 501-510.

[28] V. Sarli, A. Benedetto, E.J. Long, G.K. Hargrave, Time-resolved particle image velocimetry of dynamic interactions between hydrogen-enriched methane/air premixed flames and toroidal vortex structures, Int. J. Hydrogen Energ. 37 (2012) 16201-16213.

[29] V. Sarli, A. Benedetto, Effects of non-equidiffusion on unsteady propagation of hydrogen-enriched methane/air premixed flames, Int. J. Hydrogen Energ. 38 (2013) 7510-7518.

[30] V. Sarli, A. Benedetto, Sensitivity to the presence of the combustion submodel for large eddy simulation of transient premixed flame-vortex interactions, Ind. Eng. Chem. Res. 51 (2012) 7704-7712.

[31] E.S. Oran, V.N. Gamezo, Origins of the deflagration-to-detonation transition in gas-phase combustion, Combust. Flame 148 (2007) 4-47.

[32] G. Ciccarelli, S. Dorofeev, Flame acceleration and transition to detonation in ducts, Prog Energ Combust 34 (2008) 499-550.

[33] Y. Qi, Z. Wang, J. Wang, X. He, Effects of thermodynamic conditions on the end gas combustion mode associated with engine knock, Combust. Flame 162 (2015) 4119-4128.

[34] M. Pöschl, T. Sattelmayer, Influence of temperature inhomogeneities on knocking combustion, Combust. Flame 153 (2008) 562-573.

[35] Z. Wang, Y. Qi, X. He, J Wang, S Shuai, C.K. Law, Analysis of pre-ignition to super-knock: hotspot-induced deflagration to detonation, Fuel 144 (2015) 222-227.

[36] P. Sotiris, C. Rui, G. Dongzhi, W. Haiqiao, Experimental study on stoichiometric laminar flame velocities and Markstein lengths of methane and PRF95 dual fuels, Fuel 182 (2016) 721-731.

[37] W. Haiqiao, G. Dongzhi, Z. Lei, P. Jiaying, T. Kang, P. Zigang, Experimental observations of turbulent flame propagation effected by flame acceleration in the end gas of closed combustion chamber, Fuel 180 (2016) 157-163.

[38] L. Maley, R. Bhattacharjee, S.M. Lau-Chapdelaine, M.I. Radulescu, Influence of hydrodynamic instabilities on the propagation mechanism of fast flames, Proc. Combust. Inst. 35 (2015) 2117-2126.

[39] X. Wu, Z. Huang, X. Wang, C. Jin, C. Tang, L. Wei, C.K. Law, Laminar burning velocities and flame instabilities of 2,5-dimethylfuran-air mixtures at elevated pressures, Combust. Flame 158 (2011) 539-546.

[40] D. Bradley, C. Sheppart, R. Woolley, D. Greenhalgh, R. Lockett, The development and structure of flame instabilities and cellularity at low Markstein numbers in explosions, Combust. Flame 122 (2000) 195-209.

[41] F. Wu, G. Jomaas, C.K. Law, An experimental investigation on self-acceleration of cellular spherical flames, P Combust Inst 34 (2013) 937-945.

[42] J.D. Anderson Jr, Fundamentals of Aerodynamits, Tata McGraw-Hill Education, New York, US, 1985, p. 590.

[43] G.H. Markstein, A shock-tube study of flame front-pressure wave interaction, Proc. Combust. Inst. 6 (1957) 387-398.

[44] B.Martin, The Richtmyer-Meshkov instability, Annu.Rev.Fluid.Mech. 34(2002):445-468.

[45] S. Chaudhuri, F. Wu, D. Zhu, C.K. Law, Flame speed and self-similar propagation of expanding turbulent premixed flames, Phys Rev Lett 108 (2012) 044503.

[46] J. Zhang, Z. Sun, Y. Zheng, Z. Su, Coupling effects of foam ceramics on the flame and shock wave of gas explosion, Safety Sci. 50 (2012) 797-800.

[47] W. Jost, Explosion and combustion processes in gases, McGraw-Hill College, New York, US, 1946, p. 520.

List of Tables/Figures

Fig. 13. FFT filtered pressure for three combustion modes.

List of Supplemental Material

Video 1. Oscillating combustion at initial pressure of 2.5 bar and hole size of 3 mm.mp4

Video 2. End-gas autoignition at initial pressure of 2 bar and hole size of 1.5 mm.mp4